

RESEARCH ARTICLE

10.1002/2015JD023673

Key Points:

- First direct model comparison with multiple ground-based observations
- WAM reproduces strong summer tides and variability well
- Model enables intercomparison of different observations

Correspondence to:

R. A. Akmaev,
Rashid.Akmaev@noaa.gov

Citation:

Akmaev, R. A., J. M. Forbes, F.-J. Lübken, D. J. Murphy, and J. Höffner (2016), Tides in the mesopause region over Antarctica: Comparison of whole atmosphere model simulations with ground-based observations, *J. Geophys. Res. Atmos.*, 121, 1156–1169, doi:10.1002/2015JD023673.

Received 13 MAY 2015

Accepted 4 JAN 2016

Accepted article online 8 JAN 2016

Published online 6 FEB 2016

Tides in the mesopause region over Antarctica: Comparison of whole atmosphere model simulations with ground-based observations

R. A. Akmaev¹, J. M. Forbes², F.-J. Lübken³, D. J. Murphy⁴, and J. Höffner³
¹Space Weather Prediction Center, NOAA, Boulder, Colorado, USA, ²Department of Aerospace Engineering Sciences, University of Colorado Boulder, Boulder, Colorado, USA, ³Leibniz-Institute for Atmospheric Physics, Kühlungsborn, Germany, ⁴Australian Antarctic Division, Kingston, Tasmania, Australia

Abstract Almost a quarter century ago first optical and radar observations from the South Pole revealed rich dynamics unexpected from classical tidal theory. A strong semidiurnal wind oscillation was detected near the mesopause implying substantial deviations from the classical view that the semidiurnal variation is dominated by the migrating tide. Subsequent systematic observations exhibited large seasonal variations of both the diurnal and semidiurnal tide with dramatic reduction in amplitude from summer to winter. First numerical simulations with a realistic general circulation model extending into the lower thermosphere indicated the presence of nonmigrating tides with substantial amplitudes in the polar regions. However, direct model-data comparisons have been limited to idealized linear models. Here whole atmosphere model (WAM) simulations for January and July are compared with available wind climatologies based on multiyear radar observations at different locations in Antarctica as well as with first summertime lidar measurements of temperature. The diurnal tide simulation agrees well with most of the independent radar and satellite wind observations in both seasons. The strong semidiurnal tide comprised of migrating and nonmigrating components is well reproduced in summer, while in winter the model tends to overestimate the amplitudes over the continental edge. Besides model validation, a self-consistent numerical solution also enables cross validation of observations made with different instruments at different locales.

1. Introduction

First observations in the mesopause region over Antarctica revealed rich tidal dynamics with some unexpected features. Optical and radar measurements from the South Pole station detected occasional large-amplitude 12 h oscillations of wind and temperature in winter [Collins *et al.*, 1992; Hernandez *et al.*, 1993]. Subsequent radar observations found a persistently strong semidiurnal westward propagating tide in summer [Forbes *et al.*, 1995]. A full year of the meteor radar data showed a pronounced seasonal variation of the semidiurnal tide with maximum amplitudes in summer and minimum in winter [Portnyagin *et al.*, 1998]. Classical tidal theory commonly considered only migrating waves with the zonal phase speed following the motion of the source, which in the case of dominant thermal tides is the apparent westward motion of the Sun [Chapman and Lindzen, 1970]. Because the phase speed is the same for all migrating tides, the wave frequency in cycles per day ν equals the zonal wave number m . For the migrating semidiurnal westward tide (SW2) $\nu = m = 2$ (here and in the following an established notation of tidal waves is used [Forbes *et al.*, 2002]). However, as may be formally shown from the linearized tidal equations, the only zonal wave number corresponding to nonvanishing wind over the pole is $m = 1$ associated with an $m = 0$ variation of scalar variables such as temperature [Hernandez *et al.*, 1992].

This property of arbitrary motion over the pole seen in conventional spherical coordinates is readily understood from simple geometry. Consider a close vicinity of the pole within a latitude circle with radius $\Delta\varphi \rightarrow 0$ (Figure 1). The horizontal wind speed vector projects on the zonal U (positive eastward) and meridional V (positive northward) components. Neglecting the wind variations over this small area, it is immediately seen that along the wind direction the same wind speed projects onto positive and negative V and zero U on either side of the pole. Perpendicular to the wind direction the same wind speed corresponds to positive and negative U and zero V . On the latitude circle both components of the wind vector are of the same magnitude and antisymmetric with respect to the pole, which is formally expressed as an $m = 1$ longitudinal dependence. It is interesting to note that for a westward propagating tide (one counterclockwise rotation per period in

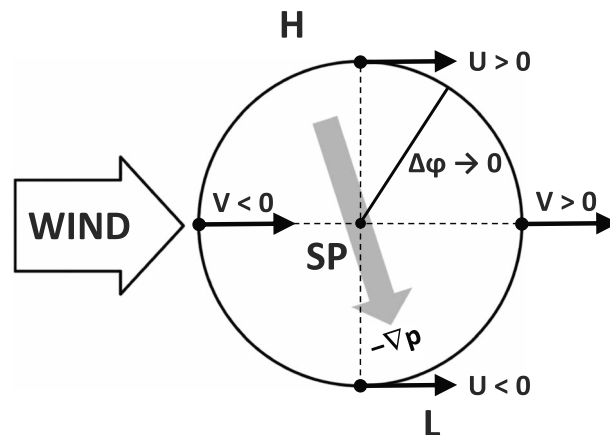


Figure 1. A schematic of arbitrary motion over the pole in spherical coordinates, with the South Pole (SP) shown for specificity. In close vicinity of the pole (within latitude distance $\Delta\phi \rightarrow 0$) the horizontal wind speed formally projects on the zonal U and meridional V components. Along the wind direction the same wind speed corresponds to positive and negative V and zero U , as shown to the right and to the left of the pole, respectively. Perpendicular to the wind direction, the same wind speed corresponds to positive and negative U and zero V , as shown above and below the pole. This implies an antisymmetric ($m = 1$) longitudinal variation of both wind components. In the Southern Hemisphere a given wind direction corresponds to high (H) and low (L) pressure (or geopotential) to the left and to the right of the wind direction, respectively. This implies an antisymmetric ($m = 1$) variation of the horizontal gradient of pressure (countergradient direction shown by the grey arrow) or $O(\Delta\phi)$ latitude dependence of the wave number 1 amplitude variation of the scalar variables themselves. With $\Delta\phi \rightarrow 0$ this corresponds to zonally symmetric (wave number 0) variation at the pole. See text for further details.

Figure 1) U reaches a maximum first, followed by a maximum of V at any longitude, i.e., U leads V in phase by a quarter period at any given longitude. Clearly, for eastward propagating tides the phase relation reverses and V leads U by a quarter period. The quarter-period phase difference between the horizontal wind components is a general property of waves in a rotating atmosphere [Gossard and Hooke, 1975]. Also, note that for a semidiurnal tide with $m = 1$ the zonal phase speed would be twice that of SW2.

In the Southern Hemisphere a given wind vector of global-scale motion corresponds to a high (H) and low (L) pressure (or geopotential) approximately to the left and to the right of the wind direction, respectively (Figure 1). [For quasi-stationary motion the wind vector is almost exactly perpendicular to the direction of pressure gradient (geostrophic wind). At tidal frequencies, which are comparable to the Coriolis parameter, the wind vector turns more in the countergradient direction (grey arrow) with increasing frequency.] This implies an $m = 1$ variation of the hori-

zonal gradient of pressure, geopotential, or of temperature in the underlying atmosphere. Neglecting the gradient vector variation in the close vicinity of the pole, it follows that the amplitude of wave number 1 variation of the scalars along the latitude circle in Figure 1 scales linearly with $\Delta\phi$ and so exactly vanishes at the pole corresponding to $m = 0$.

Radar observations in different azimuths confirmed that the strong 12 h wind oscillation was a nonmigrating westward propagating semidiurnal tide with zonal wave number $m = 1$ (SW1) [Hernandez et al., 1993; Forbes et al., 1995] prompting a search for its excitation mechanism. Of course, it should not be surprising that SW1 was observed because, as follows from the preceding discussion, $m = 1$ is the only zonal wave number that can be “seen” from the pole: the horizontal wind vector associated with arbitrary nonvanishing motion “automatically” projects on the $m = 1$ components (Figure 1). The presence of a substantial 12 h wind oscillation simply indicates that the semidiurnal tide is not symmetric with respect to the pole. Any deviation of the semidiurnal tide from the classical symmetry can be only seen from the pole as SW1. It is the magnitude of the asymmetry that was unexpected in the observations from South Pole. By comparison, the diurnal oscillation that was also observed with substantial amplitudes formally projects on the migrating diurnal tide with $v = m = 1$ (DW1); this is the only migrating tide that may be observed over the pole.

The primary generation mechanism of the diurnal and semidiurnal tides is absorption of solar radiation by water vapor in the troposphere and by ozone in the stratosphere, respectively [Chapman and Lindzen, 1970]. Clearly, the distribution of these gases as well as the background atmosphere through which the tides propagate are never zonally symmetric or stationary [e.g., Bernard, 1981; Teitelbaum and Vial, 1991; Sivkov and Shved, 1993] as assumed in classical theory [Chapman and Lindzen, 1970]. It has long been recognized that nonmigrating tides and day-to-day variations of tidal amplitudes and phases will be generated. However, initial studies extending the formalism of classical linear theory to account for nonstationary and longitudinally varying forcing and background have not predicted strong semidiurnal oscillations in the polar regions [e.g., Bernard, 1981; Teitelbaum and Vial, 1991; Sivkov and Shved, 1993].

First simulations with a more realistic general circulation model (GCM) extending into the lower thermosphere indicated substantial SW1 amplitudes in the polar regions at equinox [Miyahara and Miyoshi, 1997]. Yamashita et al. [2002] extended these simulations to a full year to evaluate the seasonal variation and identify the excitation mechanism of SW1. The GCM simulations reproduced larger amplitudes of SW1 at polar latitudes of both hemispheres in summer in general agreement with the observations in Antarctica. The global tidal phase and Eliassen-Palm diagnostics suggested propagation of SW1 from the winter hemisphere to the summer polar latitudes. Using a linear model with the background atmosphere prescribed from the yearlong GCM simulation, Yamashita et al. [2002] then tested a hypothesis that the source of SW1 enhancement in the summer hemisphere is nonlinear interaction of SW2 with a stationary planetary wave with zonal wave number 1 (SPW1) perturbation of the winter cyclonic circumpolar vortex in the opposite hemisphere. The linear model simulations qualitatively reproduced the GCM results but with significantly lower SW1 amplitudes.

A similar study by Angelats i Coll and Forbes [2002] employed a nonlinear spectral model with monthly variations of the zonal mean background and SPW1 prescribed from a combination of an empirical wind climatology and reanalysis data. Interestingly, these simulations reproduced the SW1 enhancement in the polar regions of both hemispheres during solstice but mostly above 100 km. This result is qualitatively consistent with an earlier suggestion that a weaker SW1 occasionally observed in winter may be generated by interactions of SW2 with SPW1 in the same hemisphere [Forbes et al., 1995]. Although not entirely conclusive and consistent with observations, these first mechanistic studies identified nonlinear interactions with a zonally asymmetric background atmosphere as a possible mechanism of generation and seasonal variations of SW1 observed in Antarctica [Angelats i Coll and Forbes, 2002; Yamashita et al., 2002]. Subsequent modeling [e.g., Aso, 2007] and particularly observational correlation studies [Baumgaertner et al., 2006; Smith et al., 2007; Murphy et al., 2009] solidified evidence in support of this mechanism. Additional modeling studies essentially ruled out any substantial contribution of known longitudinally varying heating sources to the observed magnitude and seasonal variation of SW1 in the polar regions [Hagan and Forbes, 2003; Zhang et al., 2010].

More recently, seasonal tidal climatologies have been compiled from multiyear observations. An upgraded meteor radar at the South Pole station provided almost continuous data for more than 2 years generally confirming the previously observed seasonal variations of SW1 and DW1 with maximum monthly mean amplitudes in summer and almost no signal in winter [Lau et al., 2006]. The semidiurnal tide was found to exhibit greater year-to-year and intraseasonal variability possibly attributable to its higher sensitivity to the background winds. Murphy et al. [2006] combined radar data from several years of observations at six stations on the "outer rim" (67–78°S) and the South Pole to create a monthly empirical climatology of diurnal and semidiurnal tidal variations of the zonal and meridional wind. Recently, Lübken et al. [2011] also estimated diurnal and semidiurnal temperature oscillations near the mesopause from 171 h of first summer optical (lidar) observations at Davis (69°S, 78°E).

There have been limited direct comparisons of observations with model simulations. Lau et al. [2006] compared monthly estimates of DW1 and SW1 from the radar observations over the pole with the simulations by a linear global-scale wave model (GSWM) [Hagan et al., 2001; Hagan and Forbes, 2003]. Good agreement in tidal amplitudes was found but only in winter when the tides are weak. Lübken et al. [2011] also obtained significantly larger tidal temperature amplitudes in summer compared to an updated version of GSWM [Zhang et al., 2010]. This study compares whole atmosphere model (WAM) simulations with the available radar observations from the South Pole [Forbes et al., 1995; Portnyagin et al., 1998], lidar observations at Davis [Lübken et al., 2011], and with an updated version of the empirical radar climatology [Murphy et al., 2006, 2009] for summer (January) and winter (July) conditions. A direct comparison facilitates the model validation. It is also well known that for a given tidal wave oscillations of different atmospheric parameters such as the wind speed and temperature, they are closely interrelated to a good approximation [e.g., Gavrilov and Dvoryashin, 1979]. Because the model solution is dynamically consistent across different locations and atmospheric variables, this comparison may also help to evaluate consistency of observations by different types of instruments and at different locations.

2. Model and Observations

WAM is a GCM extending from the surface to the exobase at a nominal mean altitude of about 600 km [Akmaev and Juang, 2008; Akmaev, 2011]. It is built from the operational weather prediction Global

Forecast System (GFS) model by extension from 64 to 150 hybrid-pressure layers in the vertical with the layer thickness of a quarter-scale height in the mesosphere and thermosphere. It incorporates appropriate physical and photochemical processes in the extended domain, including empirical models of the ionospheric plasma and electric fields [Akmaev, 2011]. Importantly for tidal generation, ozone and water vapor are globally transported with a linearized ozone photochemistry included in the middle atmosphere. Both GFS and WAM include parameterizations of unresolved “subgrid” dissipative processes affecting propagation of tides. Vertical eddy mixing resulting from instabilities of resolved motion is represented according to Louis [1979]. In the upper thermosphere molecular viscosity and heat conduction dominate [Akmaev, 2011] but do not substantially affect the dynamics near the mesopause. Wave drag by breaking orographic gravity waves originating from flow over the mountains [Palmer *et al.*, 1986; McFarlane, 1987] is also included [Kim and Arakawa, 1995].

Climatology of “free-running,” i.e., not constrained by data assimilation, WAM has been extensively validated [e.g., Akmaev, 2011; Akmaev *et al.*, 2009, 2010]. Of particular relevance to this report are studies of tides originating in the lower and middle atmosphere, including nonmigrating tides from tropical convection in the troposphere and their effects on the upper atmosphere and ionosphere [Akmaev *et al.*, 2008; Fang *et al.*, 2013; Lieberman *et al.*, 2013].

Here the model results from a free annual run of WAM similar to those analyzed before [Akmaev *et al.*, 2008; Lieberman *et al.*, 2013] are compared to three sets of available tidal observations over Antarctica. The South Pole radar (SPR) obtained daily and monthly estimates of the diurnal and semidiurnal tides in January and July in 1995–1996 [Forbes *et al.*, 1995; Portnyagin *et al.*, 1998]. The meteor radar did not resolve the signal in the vertical, and the results are attributed to a centroid height of 94 km [Murphy *et al.*, 2006]. Because the radar measures horizontal winds along the line of sight, it could only “see” the meridional component V (Figure 1). As discussed in section 1 (Figure 1), near the pole a tidal amplitude of the zonal component U should be the same and for westward tides it should lead the meridional component by a quarter period in phase. At the assumed height the sounding regions correspond to latitude of about 88°S ($\Delta\varphi \approx 2^\circ$) in the four cardinal directions in longitude [Forbes *et al.*, 1995].

Murphy *et al.* [2006] assembled several years of radar data from six stations (combining the data from the adjacent McMurdo and Scott stations) and the South Pole to develop an empirical model of monthly mean amplitudes and phases of the diurnal and semidiurnal tides at 80–94 km. Concurrent least squares fits of tidal amplitude and phase were constrained by the prescribed amplitude (latitude) and phase (longitude) variations of the fitted wave number set. Murphy *et al.* [2009] repeated the analysis using four day fits of concurrent observations from four of the six stations, yielding time series of tidal characteristics. These data have been extended to include the interval from late 2003 to mid-2011 (not continuous) providing extensive coverage of Antarctic tides. Monthly composites of these data form the climatology referred to here as the Antarctic Radar Climatology (ARC). The stations range in latitude from 68 to 78°S and so provide optimal results in that latitude band. The separation of stations in longitude limits the wave number range that can be extracted such that only three wave numbers beyond the zonally symmetric component are fitted in this analysis. Westward components with $m = 0$ –3 were thought likely to dominate the spectrum and chosen for the analysis, thus neglecting eastward propagating components. Murphy *et al.* [2006] assumed the diurnal tide to be dominated by DW1 and other wave numbers were not fitted. Here WAM simulations from the same annual run are compared to an updated version of the climatology, which now also includes westward diurnal tides with wave numbers $m = 0$ –3 and is extended down to 78 km.

Lübken *et al.* [2011] estimated diurnal and semidiurnal amplitudes and phases of temperature measured by a Fe lidar at Davis (69°S, 78°E) in January 2011. The observations were made every 1 km at 84–96 km, with the diameter of the sampling volume of about 6 m at these altitudes. Because optical observations are commonly constrained by environmental conditions such as the cloud cover and, especially during polar summer, full daylight and lowest metal densities, it is important to note that the first 171 h of observations obtained over a period of 12 days resulted in an average daily coverage of about 14.3 h per day. WAM January monthly mean tidal temperature amplitudes and phases are compared with the Davis Fe lidar (DFL) temperature observations. These comparisons should be considered preliminary and taken with caution because, given typical day-to-day dynamical variability near the mesopause and limited sampling, the observational estimates do not represent true monthly means. Additionally, because on average the data do not cover

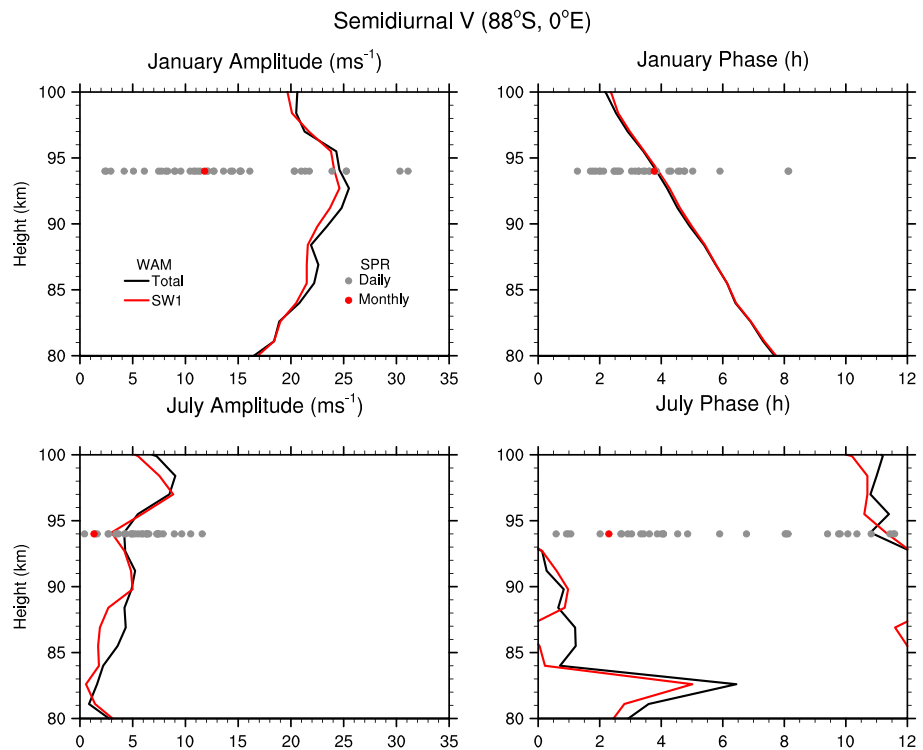


Figure 2. Comparison of semidiurnal (left column) amplitude (m s^{-1}) and (right column) phase (LT of maximum at longitude 0°) of meridional wind V (positive northward) at latitude 88°S in (top row) January and (bottom row) July as simulated by WAM (lines) and observed by the South Pole radar (SPR, dots). WAM simulations: total semidiurnal amplitude at longitude 0° (black) and the SW1 component (red). SPR observations: daily estimates (grey) and monthly average (red) of SW1 amplitude and phase.

the full 24 h period, tidal waves with different periods may alias into each other and their amplitudes may be overestimated [e.g., *Crary and Forbes, 1983; Akmaev, 1999a, 1999b*]. It may also be shown that the phase errors scale approximately inversely proportional to the wave amplitude [*Akmaev, 1999a*], meaning that in the presence of strong tides and noise the phases of weak tides cannot be determined with confidence.

3. Model-Data Comparison

Figure 2 presents daily and monthly mean amplitudes and phases of the nonmigrating semidiurnal SW1 meridional wind oscillation observed by the SPR at 94 km in January and July. Monthly mean estimates are obtained by “vector averaging” of the daily Fourier coefficients. Because Fourier transform is linear this is equivalent to Fourier analysis of a full month of data or to Fourier analysis of a monthly “average day.” The phase is defined as local time of northward maximum wind along the Greenwich meridian. Daily estimates show large variability of amplitude especially in January (up to over 30 m s^{-1}). Note that the vector averaged amplitude may equal the arithmetically averaged amplitude only if the daily phases are all exactly the same. The daily phase variations therefore result in the vector-averaged amplitudes being substantially smaller than the arithmetic averages or most of the daily values. Even in January, when the amplitudes are large, the daily phases vary within about half the period with standard deviation 1.3 h. [cf. *Murphy et al., 2006*]. Daily phases in July are essentially undefined, which is typical for phase estimates of small-amplitude waves in the presence of noise. The WAM monthly mean amplitudes and phases are shown as vertical profiles in the 80–100 km range. In January the model amplitude at 94 km ($\sim 24 \text{ m s}^{-1}$) is about twice of that observed ($\sim 12 \text{ m s}^{-1}$), while the phases ($\sim 3.5 \text{ LT}$) are in perfect agreement. Interestingly, the model amplitude profile shows a local maximum near 94 km. The model phase profile exhibits a downward phase progression with a local vertical wavelength of just over 40 km.

In July both the observations and simulations show practically a nonexistent monthly mean tide at 94 km, although the daily observational estimates extend to over 10 m s^{-1} on a few days, which is consistent with

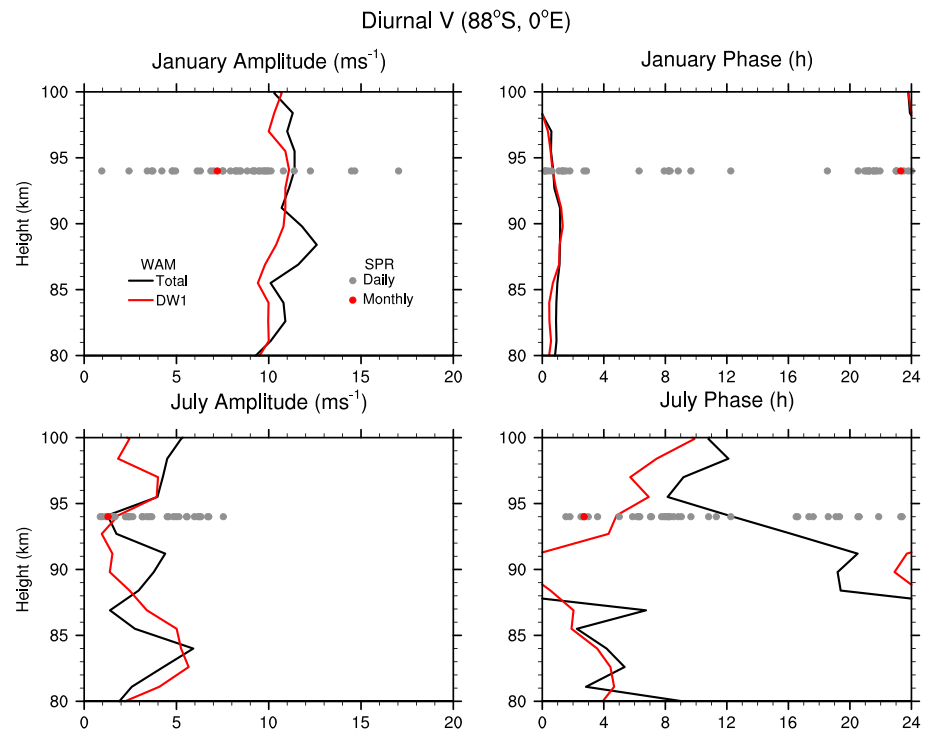


Figure 3. Same as in Figure 1 but for the diurnal tide. WAM simulations: total diurnal amplitude at longitude 0° (black) and the DW1 component (red). SPR observations: estimates for DW1.

the first observations from the pole in winter [Collins *et al.*, 1992; Hernandez *et al.*, 1993]. The observed daily phases show large variations with a standard deviation of 3.6 h, while the model phase profile exhibits large phase jumps at heights where the amplitude is minimal. In both seasons the model results are presented in two forms: as the total semidiurnal oscillation (black) at one location (88°S, 0°) and as SW1 on the latitude circle 88°S (red). As expected, both estimates are practically identical even in the case of a very weak tide in July.

The observational estimates of the migrating diurnal DW1 tide are presented in Figure 3 in a similar format. The January model amplitude at 94 km ($\sim 11 \text{ m s}^{-1}$) again substantially exceeds the observational estimate ($\sim 7 \text{ m s}^{-1}$), but the phases (near midnight) are in excellent agreement, given the standard deviation of observations of 2 h. As a wave with frequency lower than the local Coriolis parameter, the diurnal tide cannot propagate vertically at high latitudes [Chapman and Lindzen, 1970; Gossard and Hooke, 1975], which is consistent with practically a constant model phase profile in January. The SPR monthly mean amplitude is negligible and the phase is essentially undefined (standard deviation of almost 6 h) in July. The model amplitude is negligible and the phase profile exhibits characteristic irregular jumps. Observational daily estimates show a larger range of amplitude variability in January as well as substantial amplitudes on a few days in July, while the phases are highly variable in both seasons. The total diurnal oscillation at longitude 0° is practically equivalent to DW1 in the simulations as expected (Figure 1).

Figures 4–7 show similar comparisons for the semidiurnal and diurnal oscillations of both wind components with an updated ARC model, in which the monthly means are available at 78–94 km decomposed into westward propagating waves with $m = 0–3$. The amplitudes and phases are given for latitude 69°S and longitude 0°. Figure 4 compares the semidiurnal amplitudes and phases of the meridional wind component V corresponding to the different wave numbers. In January there is good agreement in amplitudes of the largest tides SW2, S0, and SW1, the latter two also being consistent with satellite observations of nonmigrating semidiurnal tides [Iimura *et al.*, 2009]. The simulations also show a very weak SW3 but the observational amplitude of $1–4 \text{ m s}^{-1}$ is likely at the noise level. In July the model overestimates the SW2 and SW1 amplitudes compared to the climatology (Figure 4), with weak amplitudes of the other components in both simulations and observations. It has been noted before that WAM tends to overestimate the amplitude of the semidiurnal

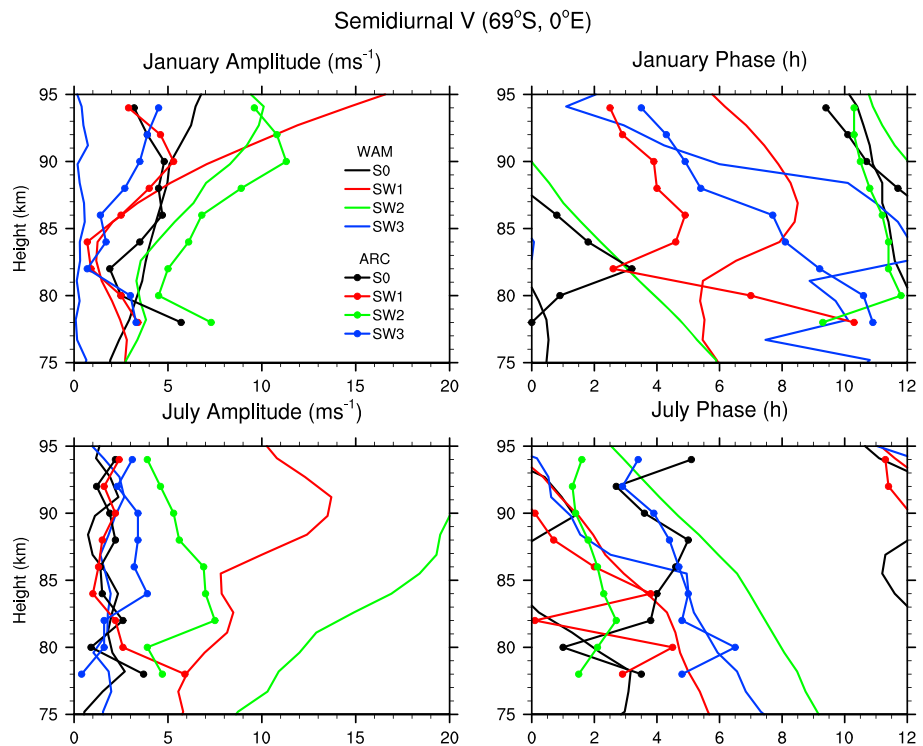


Figure 4. Same as in Figure 2 but for an updated empirical Arctic radar climatology (ARC) at 69°S and 0° longitude. Largest semidiurnal components: S0 (black), SW1 (red), SW2 (green), and SW3 (blue).

tide in winter [e.g., Akmaev et al., 2008; Pedatella et al., 2014]. This is most likely related to the overestimation of the zonal mean eastward winds in the middle atmosphere of the winter hemisphere (see also section 4).

The simulations and observations of the semidiurnal oscillation of the zonal wind (Figure 5) are generally consistent with the results presented for the meridional wind (Figure 4). The amplitudes of SW2 and SW1 simulated and observed in January are consistent and comparable with those of the meridional wind component. The radar observations show a somewhat higher S0 amplitude at 85–90 km than the WAM simulation, the ARC meridional wind amplitude (Figure 4) or satellite observations [Jimura et al., 2009]. In July SW2 is again the strongest tide in the observations and simulations with the model substantially overestimating both SW2 and SW1.

In January there is reasonable agreement in the phases of SW2 and S0 of the meridional and zonal wind components (Figures 4 and 5), both indicating vertical propagation, except near the bottom of the layer where the amplitudes are small and the observations show large phase jumps. The observations indicate a somewhat longer vertical wavelength for SW2 in both seasons. Unlike at the pole (Figure 2), SW1 becomes a minor component below about 90 km in both observations and simulations in January (Figures 4 and 5). While the observations appear to indicate vertical phase progression of SW1 in the whole layer but with some large jumps near the bottom, the model only shows a phase profile tilt above 90 km; at lower altitudes the phase becomes ill defined. The phases of the strongest semidiurnal harmonics of zonal wind lead the meridional wind phases by about a quarter period as expected [Gossard and Hooke, 1975].

A new feature of the updated ARC is the addition of wave numbers 0, 2, and 3 to the decomposition of the diurnal tide (Figures 6 and 7). This does not change the earlier conclusion that DW1 is the dominant diurnal oscillation over the entire continent during summer [Murphy et al., 2006]. In January the simulations closely reproduce the observations of DW1 amplitude and phase (Figures 6 and 7). As expected, the amplitudes of both wind components are very close and the zonal wind oscillation leads by about a quarter period in phase (Figure 1); the phase is also practically constant with altitude. In winter all diurnal components are weak with typically irregular phase profiles, except perhaps for DW1 in the WAM simulation showing a weak amplitude maximum ($\sim 6\text{--}7\text{ m s}^{-1}$) and the same phase as in summer for both V and U near 80 km.

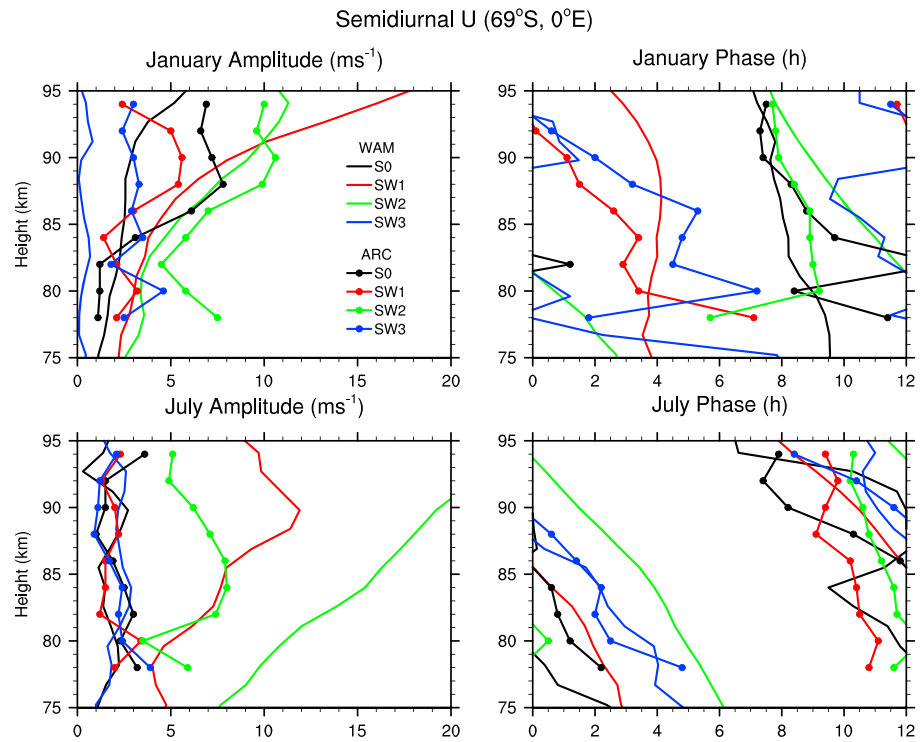


Figure 5. Same as in Figure 4 but for the zonal wind U (positive eastward).

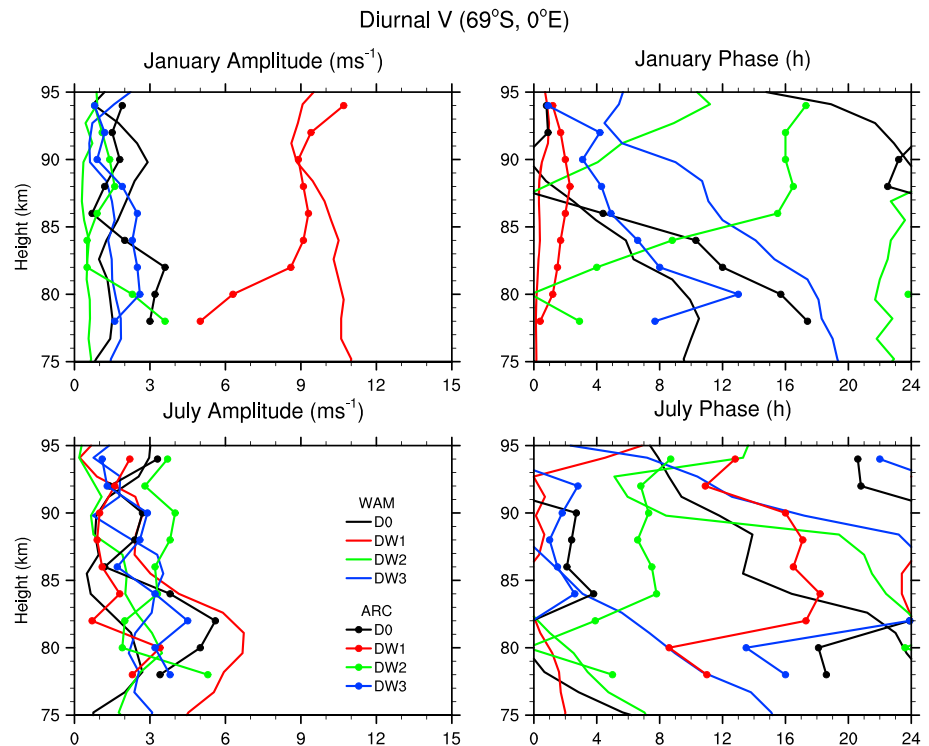


Figure 6. Same as in Figure 4 but for the diurnal tide. Largest diurnal components at longitude 0°: D0 (black), DW1 (red), DW2 (green), and DW3 (blue).

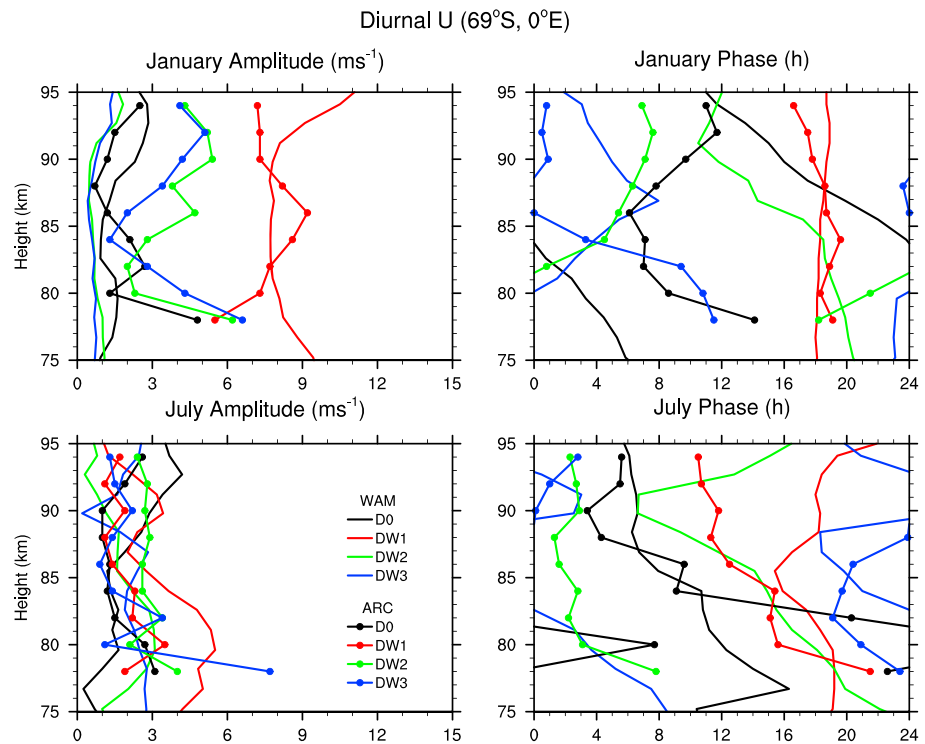


Figure 7. Same as in Figure 6 but for zonal wind U .

Figure 8 compares the monthly mean diurnal and semidiurnal tidal amplitudes of temperature simulated by WAM in January with the DFL observations over 12 days during 11–28 January 2011 [Lübken *et al.*, 2011]. The observations are available every kilometer between 84 and 96 km. Lübken *et al.* [2011] also provide error estimates shown as ± 1 standard error and accounting for instrumental errors (1–3 K with 1 h integration) and natural variability (~ 10 K). As suggested above, this comparison should be considered preliminary and taken with caution because the average local time coverage during the 12 days is only 14.3 h per day. Given the large natural variability, instrumental error, and limited sampling, estimation of the tidal amplitudes and phases, as well as their errors may not be entirely straightforward [Crary and Forbes, 1983; Akmaev, 1999a, 1999b].

WAM simulations show a fast-growing amplitude of the total diurnal oscillation above 85 km, intersecting the observations at about 90 km. Below this level the observations show a larger amplitude of about 3–4 K. Above about 93 km the total simulated tide is dominated by DW1 and the total tidal phase closely matches the phase of that component, which is approximately constant with height. Below 90 km the simulated total tide and all its components become weak compared to the observations, the two largest being DW1 and DE1 (Figure 8). Near 84 km these two tides are nearly in antiphase, the total amplitude becomes small and the total phase exhibits a large jump. Near 80 km it approaches the phase of DE1. Lübken *et al.* [2011] suggest that there may be a downward progression of the diurnal phase corresponding to a vertical wavelength of about 30 km. This conclusion depends on how reliable the phase estimates at individual heights are. If, for example, the two highest points (95 and 96 km) are eliminated, then the observed phase profile will not show a phase progression and be consistent with the simulations. Note that the large phase jump near the top of the profile corresponds to the minimum amplitude observed. Conversely, if the observations at 93–94 km are excluded, the profile appears to support the conclusion of Lübken *et al.* [2011]. Theoretically, the diurnal tide cannot propagate vertically at high latitudes [Chapman and Lindzen, 1970], as is also seen in the wind observations and simulations presented above.

The observed profile of the semidiurnal amplitude “oscillates” around the model profile of total semidiurnal oscillation showing a better agreement than the diurnal amplitude. Up to 97 km the simulated semidiurnal oscillation almost entirely consists of SW1 with smaller and roughly equal contributions from SW2 and S0.

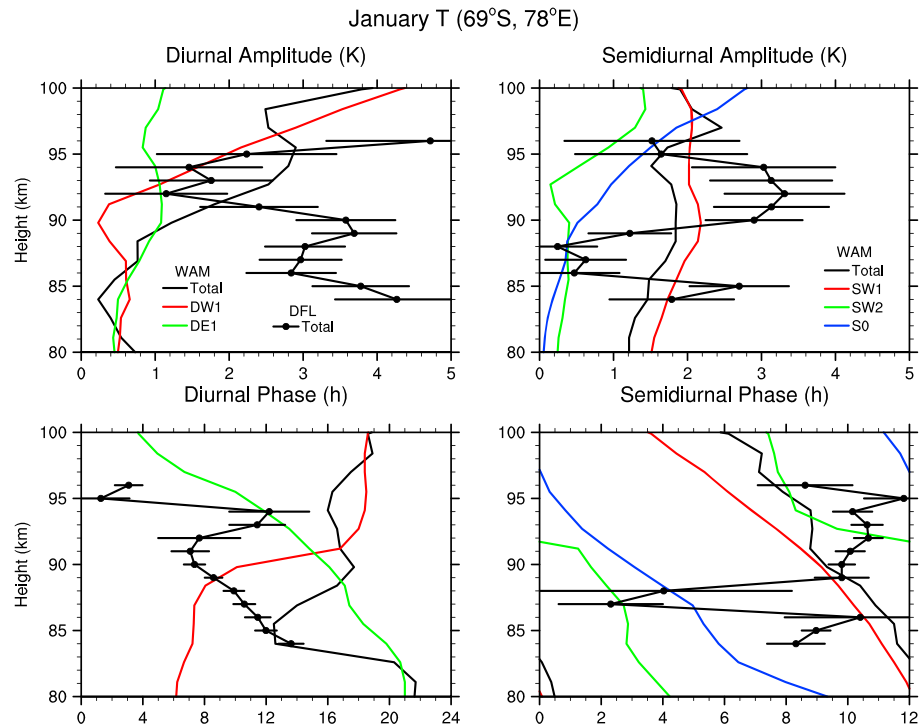


Figure 8. Comparison of (left column) diurnal and (right column) semidiurnal temperature (top row) amplitude (K) and (bottom row) phase (LT of maximum) over Davis (69°S, 78°E) as simulated by WAM and observed by the lidar (DFL) in January. WAM simulations: total (black) and the largest tidal components (left column) DW1 (red) and DE1 (green); and (right column) SW1 (red), SW2 (green), and S0 (blue).

The total simulated phase closely follows that of SW1 and is in reasonable agreement with the observed phase profile, which is approximately constant with altitude, if a large jump around 87–88 km corresponding to a local amplitude minimum is neglected. On the other hand, all the simulated components shown exhibit a downward phase propagation corresponding to local vertical wavelengths in the range of about 20–40 km, also consistent with the wind observations and simulations. Note again, that the semidiurnal tides can propagate vertically at these latitudes [Chapman and Lindzen, 1970]. Overall, this preliminary comparison shows some similarities and some differences between the simulations and observations.

4. Discussion

The model-data comparisons presented in the previous section show excellent agreement of the simulations with observations at some locations and in some seasons as well as some discrepancies. Because the model solution is dynamically self consistent, this generally implies that the observations taken by different instruments and at different locales may not be consistent with each other regardless of whether the model is correct or not.

Analyzing a few years of observations with an upgraded meteor radar at the South Pole, Lau et al. [2006] note that despite substantial seasonal variations, the diurnal and semidiurnal monthly mean phases are highly repeatable from year to year, especially during summer. The good agreement of the model phases with the SPR observations (Figures 2 and 3) and with those of Lau et al. is encouraging. WAM simulations of the diurnal tide also show excellent agreement in amplitude and phase of both wind components with the updated radar climatology at 78–94 km, indicating that in summer the tide is dominated by the migrating DW1 component (Figures 6 and 7). Lau et al. [2006] estimate the DW1 amplitude at about 10 m s^{-1} between 87.5–97.5 km at the pole in January 2002 and 2003 also in excellent agreement with the simulations (Figure 3). The agreement of DW1 simulated by WAM with the multiyear radar observations over the whole continent assures confidence and is consistent with the independent model validation by multiyear satellite observations of seasonal variations of DW1 in temperature at middle and low latitudes [Akmaev et al., 2008].

At the same time the model diurnal amplitude substantially exceeds the SPR wind observations at 94 km (Figure 3). The smaller diurnal amplitude obtained in the radar observations may possibly be explained by the fact that the monthly mean presented here was constructed from parts of the month of January in two different years (1995 and 1996) as well as by large daily variability during the specific periods of observation (Figure 3). It should also be noted that subsequent SPR observations in January 1997 are more consistent with the other observations and WAM simulations [Forbes *et al.*, 1999]. On the other hand, the DFL temperature observations at 69°S show a substantially larger diurnal amplitude of temperature than that simulated below 90 km in January (Figure 8). It is interesting to contrast here that the ARC monthly mean diurnal amplitudes for both wind components are either slightly smaller (Figure 6) or very close (Figure 7) to the WAM simulations at these altitudes and latitude in January. As already mentioned the limited number of days available and uneven daily coverage in the presence of large natural variability (~ 10 K) in the DFL data [Lübken *et al.*, 2011] may substantially affect the estimation of amplitudes and phases of harmonic oscillations as well as their errors [Crary and Forbes, 1983; Akmaev, 1999a, 1999b].

Of course, the large dynamical variability is not limited to the lidar observations but has been seen in other observations near the mesopause as well [e.g., Murphy *et al.*, 2006] reflecting the effects of realistic variable sources and background conditions on propagation of tides [Bernard, 1981; Teitelbaum and Vial, 1991; Sivkov and Shved, 1993]. Figures 2 and 3, for example, show large daily variability of the daily estimates of tidal amplitudes and phases obtained from the SPR observations. Unlike climatological models as GSWM [Hagan *et al.*, 2001; Zhang *et al.*, 2010], WAM, built on a weather prediction model, realistically reproduces “tidal weather” seen in tremendous daily variations of tidal amplitudes of all the variables at the same geographic locations as presented in the previous section (e.g., Figures 2 and 3). Figure 9 shows similar variability of simulated daily amplitudes of the wind components and temperature at the locations considered in this study. Note again that the vector-averaged amplitude may equal the arithmetically averaged amplitude only if the daily phases are all exactly the same. The daily phase variations arising, e.g., from nonlinear interactions with the background and other waves [Bernard, 1981; Teitelbaum and Vial, 1991], therefore result in the vector-averaged amplitudes being substantially smaller than the arithmetic averages. This explains why the monthly mean amplitudes are substantially smaller than most of the daily values in Figure 9. The comparison presented in Figure 8 should therefore be seen as demonstration of capability of the model to “bridge” observations by different instruments at different locales. Clearly more lidar data with better local time coverage is necessary for a more rigorous evaluation.

In January the semidiurnal amplitude simulated by WAM exceeds that observed by SPR at 94 km by about a factor of 2 (Figure 2). Based on a few years of observations from the pole, Lau *et al.* [2006] note large interannual variations of the semidiurnal amplitudes in summer months reaching values of up to $20\text{--}30\text{ ms}^{-1}$ between 90 and 100 km, which is close to the WAM estimates (Figure 2). Perhaps the relatively low January mean amplitude observed by SPR (Figure 2) may be partially attributed to a specific period of observations. The WAM amplitudes are in reasonable agreement with the ARC multiyear estimate for the leading semidiurnal tides of both wind components on the outer rim (Figures 4 and 5), at least up to about 90 km for SW1, which is the only semidiurnal tide seen from the pole. There is also reasonable agreement with the DFL temperature observations at 84–96 km (Figure 8) given the large daily variability and undersampling of the optical observations. Note that in principle, shorter-period oscillations such as semidiurnal may be recovered with greater confidence from partial-day data than longer-period ones such as diurnal [Akmaev, 1999a, 1999b]. This may partially explain a better agreement of simulations of the semidiurnal tide with the lidar observations (Figure 8).

In July WAM overestimates the amplitudes of SW1 and SW2 compared to the ARC amplitudes at 69°S (Figures 4 and 5). As mentioned above, this is most likely related to the sensitivity of the semidiurnal tide to the background zonal mean wind. WAM may overestimate the eastward zonal mean winds in the winter middle atmosphere, especially in the Southern Hemisphere. Current work to improve parameterization of nonorographic gravity waves in WAM should help to alleviate this bias. Preliminary experiments show that the additional wave drag reduces the eastward zonal mean wind and brings the semidiurnal amplitudes closer to observations in the winter hemisphere (V. A. Yudin, personal communication, 2015). Characteristically, the amplitudes of SW1 and SW2 propagating against the strong background eastward wind in the winter simulations even exceed those in summer, at least below 90 km (Figures 4 and 5). Yet over the pole the WAM amplitude of SW1 is substantially lower in winter than in summer (Figure 2), which is consistent, at least qualitatively, with all radar wind observations from the pole [Lau *et al.*, 2006].

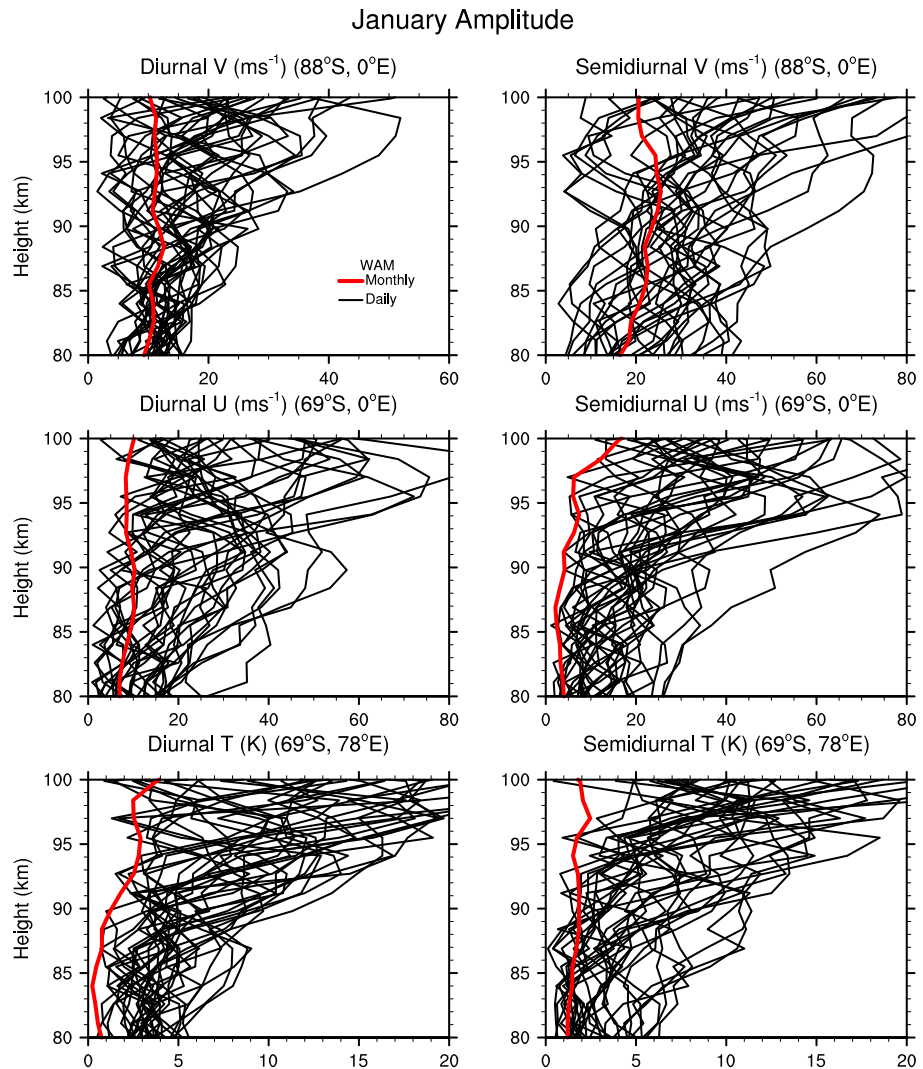


Figure 9. January daily (black) and monthly mean (red) amplitude of (left column) diurnal and (right column) semidiurnal oscillation of (top row) meridional wind at (88°S, 0°E), (middle row) zonal wind at (69°S, 0°E), and (bottom row) temperature over Davis (69°S, 78°E) as simulated by WAM at 80–100 km.

It is interesting to compare the tidal amplitudes of the meridional wind at the pole and the outer rim because one of the empirical ARC fits to the observations assumed constant amplitudes and phases based on the altitudinal variation of a few gravest Hough modes for the $m = 1$ tides [Murphy *et al.*, 2006]. In an alternative fit using only the outer rim radar data Murphy *et al.* [2006] obtained amplitudes even lower than observed by the SPR in summer, which in turn appear underestimated [Lau *et al.*, 2006]. This means that the assumption of constant tide may not be valid for SW1 in summer. It is not supported by either the WAM simulations (cf. Figures 2 and 4) or other observations in the polar region [Iimura *et al.*, 2009] possibly because of higher-order semidiurnal Hough modes present. The tide essentially becomes more symmetric away from the pole, with substantial contributions from SW2 and S0 to the total semidiurnal power at 69°S. Conversely, in winter the model appears to show a larger amplitude of SW1 on the outer rim than at the pole (Figures 2 and 4), for reasons just discussed. The assumption of a constant SW1 tide between 69°S and the South Pole does not appear to be satisfied in either season.

Interestingly, the WAM simulations appear to be consistent with the assumption of constant amplitude and phase of DW1 over the whole continent at least for the meridional wind component (Figures 3 and 6). This is also consistent with other radar observations [Lau *et al.*, 2006] and may be related to the fact that unlike the semidiurnal tide the diurnal tide in summer is dominated by DW1 according to both observations and

simulations. Another assumption that may potentially affect the ARC analysis [Murphy *et al.*, 2006] is fitting to the data only the westward tidal components with zonal wave numbers $m=0-3$. According to WAM simulations (not shown), there may be nonnegligible spectral power in the eastward tidal components with the same wave numbers, which may potentially affect the results especially for relatively weak tides.

5. Conclusion

First observations from the South Pole revealed rich and unexpected tidal dynamics with large seasonal and daily variability near the mesopause. Direct validation of WAM simulations with multiyear radar wind climatologies as well as with the first summertime lidar temperature observations suggests that overall the model adequately represents the dominant components of the tidal spectrum over Antarctica. The diurnal migrating DW1 amplitude and phase are reproduced by the model in excellent agreement with the majority of independent wind observations over the whole continent during the seasons of "high tide" and "low tide."

The semidiurnal wind oscillation may only be seen from the pole as nonmigrating SW1, meaning that the tide is no longer symmetric. It is simulated in reasonable agreement with the radar climatologies during the summer "high tide" season. The model appears to substantially overestimate the semidiurnal tide in winter over the continental rim, where it contains large contributions from the migrating SW2 and nonmigrating S0 components. Future work will be aimed at better representation of the wintertime zonal mean background climatology in WAM most likely causing the overestimation.

The model dynamically self-consistent solution offers a framework for cross validation of observations of different atmospheric parameters made by different instruments or at different locations. Clearly, if the model agrees with some observations and disagrees with others or if it disagrees with the different observations but in a different sense, these data sets may not be mutually consistent, whether the model is correct or not. A realistic numerical simulation also facilitates evaluation of some simplifying assumptions based on classical linear theory and used in construction of empirical climatologies. For example, both the simulations and observations imply that the assumption of constant amplitudes and phases for SW1 is not quite justified between the outer rim and the South Pole possibly indicating the presence of higher-order Hough modes. The diurnal tidal wind oscillation, on the other hand, appears to be consistent with this assumption suggesting that the dominating DW1 is primarily comprised of the gravest Hough modes.

Previous observations have concentrated on the diurnal and semidiurnal tides. In future work it would also be interesting to estimate possible contribution of higher-frequency oscillations such as the terdiurnal tide to the overall tremendous dynamical variability seen in both the observations and simulations over Antarctica.

Acknowledgments

J.M.F. acknowledges support under NASA award NNX12AJ58G as part of the Heliophysics Guest Investigator Program. The MF radar at Rothera is a joint project between the British Antarctic Survey (BAS) and GATS Inc. operated by BAS. Support through NSF grant OPP-0839084 is acknowledged along with the assistance of David Fritts. The Scott Base MF radar is operated by Adrian McDonald and colleagues at the University of Canterbury through Antarctica New Zealand. Syowa MF radar operation has been carried out by Masaki Tsutsumi, National Institute of Polar Research under the Japanese Antarctic Research Expeditions (JAREs). The Davis and Mawson MF radars are supported through the Australian Antarctic Program through grant 674, and the assistance of Robert Vincent is acknowledged. The IDI radar at Halley was owned and operated by BAS and the assistance of Andrew Kavanagh and his colleagues is acknowledged. Computational resources were provided by the NOAA R&D high performance computing system. The tidal analysis results presented here are stored on this system and are available upon request (Rashid.Akmaev@noaa.gov).

References

- Akmaev, R. A. (1999a), A prototype upper-atmospheric data assimilation scheme based on optimal interpolation: 1. Theory, *J. Atmos. Sol. Terr. Phys.*, **61**, 491–504.
- Akmaev, R. A. (1999b), A prototype upper-atmospheric data assimilation scheme based on optimal interpolation: 2. Numerical experiments, *J. Atmos. Sol. Terr. Phys.*, **61**, 505–517.
- Akmaev, R. A. (2011), Whole atmosphere modeling: Connecting terrestrial and space weather, *Rev. Geophys.*, **49**, RG4004, doi:10.1029/2011RG000364.
- Akmaev, R. A., and H.-M. H. Juang (2008), Using enthalpy as a prognostic variable in atmospheric modelling with variable composition, *Q. J. R. Meteorol. Soc.*, **134**, 2193–2197.
- Akmaev, R. A., T. J. Fuller-Rowell, F. Wu, J. M. Forbes, X. Zhang, A. F. Anghel, M. D. Iredell, S. Moorthi, and H.-M. H. Juang (2008), Tidal variability in the lower thermosphere: Comparison of Whole Atmosphere Model (WAM) simulations with observations from TIMED, *Geophys. Res. Lett.*, **35**, L03810, doi:10.1029/2007GL032584.
- Akmaev, R. A., F. Wu, T. J. Fuller-Rowell, and H. Wang (2009), Midnight temperature maximum (MTM) in Whole Atmosphere Model (WAM) simulations, *Geophys. Res. Lett.*, **36**, L07108, doi:10.1029/2009GL037759.
- Akmaev, R. A., F. Wu, T. J. Fuller-Rowell, H. Wang, and M. D. Iredell (2010), Midnight density and temperature maxima, and thermospheric dynamics in Whole Atmosphere Model simulations, *J. Geophys. Res.*, **115**, A08326, doi:10.1029/2010JA015651.
- Angelats i Coll, M., and J. M. Forbes (2002), Nonlinear interactions in the upper atmosphere: The $s=1$ and $s=3$ nonmigrating semidiurnal tides, *J. Geophys. Res.*, **107**(A8), 1157, doi:10.1029/2001JA900179.
- Aso, T. (2007), A note on the semidiurnal non-migrating tide at polar latitudes, *Earth Planets Space*, **59**, e21–e24.
- Baumgaertner, A. J. G., M. J. Jarvis, A. J. McDonald, and G. J. Fraser (2006), Observations of the wavenumber 1 and 2 components of the semi-diurnal tide over Antarctica, *J. Atmos. Sol. Terr. Phys.*, **68**, 1195–1214.
- Bernard, R. (1981), Variability of the semi-diurnal tide in the upper mesosphere, *J. Atmos. Terr. Phys.*, **43**, 663–674.
- Chapman, S., and R. S. Lindzen (1970), *Atmospheric Tides: Thermal and Gravitational*, D Reidel Publ., Dordrecht.
- Collins, R. L., D. C. Senft, and C. S. Gardner (1992), Observations of a 12 h wave in the mesopause region at the South Pole, *Geophys. Res. Lett.*, **19**, 57–60, doi:10.1029/91GL02780.

- Crary, D. J., and J. M. Forbes (1983), On the extraction of tidal information from measurements covering a fraction of a day, *Geophys. Res. Lett.*, **10**, 580–582, doi:10.1029/GL010i007p00580.
- Fang, T.-W., R. A. Akmaev, T. Fuller-Rowell, F. Wu, N. Maruyama, and G. Millward (2013), Longitudinal and day-to-day variability in the ionosphere from lower atmosphere tidal forcing, *Geophys. Res. Lett.*, **40**, 2523–2528, doi:10.1002/grl.50550.
- Forbes, J. M., N. A. Makarov, and Y. I. Portnyagin (1995), First results from the meteor radar at South Pole: A large 12-h oscillation with zonal wavenumber one, *Geophys. Res. Lett.*, **22**, 3247–3250, doi:10.1029/95GL03370.
- Forbes, J. M., Y. I. Portnyagin, N. A. Makarov, S. E. Palo, E. G. Merzlyakov, and X. Zhang (1999), Dynamics of the lower thermosphere over South Pole from meteor radar wind measurements, *Earth Planets Space*, **51**, 611–620.
- Forbes, J. M., A. F. C. Bridger, S. W. Bougher, M. E. Hagan, J. L. Hollingsworth, G. M. Keating, and J. Murphy (2002), Nonmigrating tides in the thermosphere of Mars, *J. Geophys. Res.*, **107**(E11), 5113, doi:10.1029/2001/JE001582.
- Gavrilov, N. M., and S. V. Dvoryashin (1979), Estimates of the tidal parameters in the upper atmosphere from radio meteor measurements: Application to [OI] 5577 Å emission, *Geomagn. Aeron. (English Trans.)*, **19**, 243–244.
- Gossard, E. E., and W. H. Hooke (1975), *Waves in the Atmosphere*, Elsevier, Amsterdam.
- Hagan, M. E., and J. M. Forbes (2003), Migrating and nonmigrating semidiurnal tides in the upper atmosphere excited by tropospheric latent heat release, *J. Geophys. Res.*, **108**(A2), 1062, doi:10.1029/2002JA009466.
- Hagan, M. E., R. G. Roble, and J. Hackney (2001), Migrating thermospheric tides, *J. Geophys. Res.*, **106**(A7), 12,739–12,752, doi:10.1029/2000JA000344.
- Hernandez, G., R. W. Smith, G. J. Fraser, and W. L. Jones (1992), Large-scale waves in the upper-mesosphere at Antarctic high-latitudes, *Geophys. Res. Lett.*, **19**, 1348–1350.
- Hernandez, G., G. I. Fraser, and R. W. Smith (1993), Mesospheric 12-hour oscillation near South Pole, Antarctica, *Geophys. Res. Lett.*, **20**, 1787–1790, doi:10.1029/93GL01983.
- Imura, H., S. E. Palo, Q. Wu, T. L. Killeen, S. C. Solomon, and W. R. Skinner (2009), Structure of the nonmigrating semidiurnal tide above Antarctica observed from the TIMED Doppler Interferometer, *J. Geophys. Res.*, **114**, D11102, doi:10.1029/2008JD010608.
- Kim, Y.-J., and A. Arakawa (1995), Improvement of orographic gravity wave parameterization using a mesoscale gravity wave model, *J. Atmos. Sci.*, **52**, 1875–1902.
- Lau, E. M., S. K. Avery, J. P. Avery, S. E. Palo, and N. A. Makarov (2006), Tidal analysis of meridional winds at the South Pole using a VHF interferometric meteor radar, *J. Geophys. Res.*, **111**, D16108, doi:10.1029/2005JD006734.
- Lieberman, R. S., R. A. Akmaev, T. J. Fuller-Rowell, and E. Doornbos (2013), Thermospheric zonal mean winds and tides revealed by CHAMP, *Geophys. Res. Lett.*, **40**, 2439–2443, doi:10.1002/grl.50481.
- Louis, J.-F. (1979), A parametric model of vertical eddy fluxes in the atmosphere, *Boundary Layer Meteorol.*, **17**, 187–202.
- Lübken, F.-J., J. Höffner, T. P. Viehl, B. Kaifler, and R. J. Morris (2011), First measurements of thermal tides in the summer mesopause region at Antarctic latitudes, *Geophys. Res. Lett.*, **38**, L24806, doi:10.1029/2011GL050045.
- McFarlane, N. A. (1987), The effect of orographically excited gravity wave drag on the general circulation of the lower stratosphere and troposphere, *J. Atmos. Sci.*, **44**, 1775–1800.
- Miyahara, S., and Y. Miyoshi (1997), Migrating and nonmigrating atmospheric tides simulated by a middle atmosphere general circulation model, *Adv. Space Res.*, **20**, 1201–1207.
- Murphy, D. J., et al. (2006), A climatology of tides in the Antarctic mesosphere and lower thermosphere, *J. Geophys. Res.*, **111**, doi:10.1029/2005JD006803.
- Murphy, D. J., T. Aso, D. C. Fritts, R. E. Hibbins, A. J. McDonald, D. M. Riggan, M. Tsutsumi, and R. A. Vincent (2009), Source regions for Antarctic MLT non-migrating semidiurnal tides, *Geophys. Res. Lett.*, **36**, L09805, doi:10.1029/2008GL037064.
- Palmer, T. N., G. J. Shutts, and R. Swinbank (1986), Alleviation of a systematic westerly bias in general circulation and numerical weather prediction models through an orographic gravity wave drag parameterization, *Q. J. R. Meteorol. Soc.*, **112**, 1001–1039.
- Pedatella, N. M., et al. (2014), The neutral dynamics during the 2009 sudden stratosphere warming simulated by different whole atmosphere models, *J. Geophys. Res. Space Physics*, **119**, 1306–1324, doi:10.1002/2013JA019421.
- Portnyagin, Y. I., J. M. Forbes, N. A. Makarov, E. G. Merzlyakov, and S. Palo (1998), The summertime 12-h wind oscillation with zonal wave-number $s = 1$ in the lower thermosphere over the South Pole, *Ann. Geophys.*, **16**, 828–837.
- Sivkov, A. M., and G. M. Shved (1993), Influence of latitudinal and longitudinal variations of ozone and water vapour on the solar semidiurnal tide, *J. Atmos. Terr. Phys.*, **55**, 815–826.
- Smith, A. K., D. V. Pancheva, N. J. Mitchell, D. R. Marsh, J. M. Russell, and M. G. Mlynczak (2007), A link between variability of the semidiurnal tide and planetary waves in the opposite hemisphere, *Geophys. Res. Lett.*, **34**, L07809, doi:10.1029/2006GL028929.
- Teitelbaum, H., and F. Vial (1991), On tidal variability induced by nonlinear interaction with planetary waves, *J. Geophys. Res.*, **96**, 14,169–14,178, doi:10.1029/91JA01019.
- Yamashita, K., S. Miyahara, Y. Miyoshi, K. Kawano, and J. Ninomiya (2002), Seasonal variation of non-migrating semidiurnal tide in the polar MLT region in a general circulation model, *J. Atmos. Sol. Terr. Phys.*, **64**, 1083–1094.
- Zhang, X., J. M. Forbes, and M. E. Hagan (2010), Longitudinal variation of tides in the MLT region: 2. Relative effects of solar radiative and latent heating, *J. Geophys. Res.*, **115**, A06317, doi:10.1029/2009JA014898.